

Spatiotemporal Oscillations and Rheochaos in a Simple Model of Shear Banding

S. M. Fielding* and P. D. Olmsted

Polymer IRC and School of Physics & Astronomy, University of Leeds, Leeds LS2 9JT, United Kingdom
(Received 28 October 2003; published 24 February 2004)

We study a simple model of shear banding in which the flow-induced phase is destabilized by coupling between flow and microstructure (wormlike micellar length). By varying the strength of instability and the applied shear rate, we find a rich variety of oscillatory and chaotic shear banded flows. At low shear and weak instability, the induced phase pulsates next to one wall of the flow cell. For stronger instability, high shear pulses ricochet across the cell. At high shear we see oscillating bands on either side of central defects. We discuss our results in the context of recent experiments.

DOI: 10.1103/PhysRevLett.92.084502

PACS numbers: 47.50.+d, 47.20.-k, 47.52.+j, 47.54.+r

Complex fluids commonly undergo flow instabilities and flow-induced phase transitions that result in spatially heterogeneous “shear banded” states. Classically studied systems include wormlike micellar surfactants [1], dense lamellar onion [2] or cubic [3] phases, and polymer solutions [4]. Fluidity banding has also been reported in soft glassy materials [5] such as colloidal suspensions [6] and simulated Lennard Jones particles [7]. Experimentally, the basic observation is of two coexisting shear bands with differing viscosity and microstructure (or fluidity). Theoretically, this is captured by invoking multiple flow branches in the constitutive relation of shear stress versus shear rate, $\Sigma(\dot{\gamma})$ [8–10]. The system then separates into a steady state comprising two shear bands, each on its own flow branch [Fig. 1(a)].

However an accumulating body of data shows this basic picture to be oversimplified: Many shear banding systems display *oscillations* or *irregular fluctuations suggesting chaos* in their bulk rheology, rheo-optics, or velocimetry. Example systems include onion phases [11]; shear thinning wormlike micelles (WMs) with a stress plateau in the flow curve [12], showing common stress banding (band normals in the flow-gradient direction) [13,14]; shear thickening WMs showing common stress [15] or common strain rate (vorticity) [16] banding; and polymer solutions [4]. Erratic stress response has also been studied in dense colloidal suspensions [17]. In contrast, the present models predict steady banded states [8–10].

In the noninertial limit relevant to these materials, the nonlinearity underlying this erratic response must arise in the constitutive behavior of the system [18]. Temporal “rheochaos” has been studied in homogeneous models of both director dynamics in sheared nematics [19] and shear thickening systems with a single-branched flow curve [18]. In many systems, however, heterogeneity is likely to be a crucial ingredient of rheochaos. Motivated by the above experiments, we introduce the first model of spatiotemporal rheochaos in shear banding systems with multibranched constitutive curves.

Homogeneous flow is unstable in any region of negative constitutive slope, $d\Sigma/d\dot{\gamma} < 0$. This is easily seen in models that take the “mechanical variables” (Σ , $\dot{\gamma}$) as the relevant dynamic variables [20]. The system can then separate into two shear bands, each on its own stable flow branch. See Fig. 1(a) for shear thinning gradient-banding systems. In more realistic models, the mechanical variables are coupled to microstructural quantities such as director orientation [8], polymeric concentration [21], or micellar length [22]. This coupling can destabilize the rising high shear branch and cause, e.g., tumbling and wagging in nematics [23]. Here we construct a simple model with an unstable high shear branch [Figs. 1(b) and 1(c)] and show that it has oscillatory and chaotic shear banded states at imposed global shear rate. Our model resembles other globally coupled reaction diffusion systems [24]. Aradian and Cates are currently studying spatiotemporal flows of similar models with a single constitutive branch [25].

We use only the minimal ingredients needed to capture the observed phenomena, so we do not address the

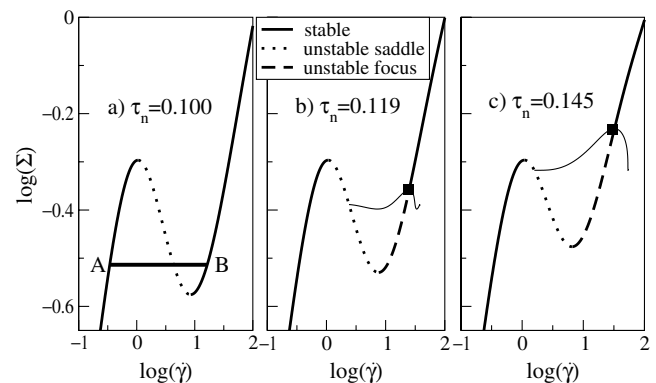


FIG. 1. Intrinsic constitutive curves for differing degrees of coupling between flow and micellar length. (a) Weak coupling, giving the standard coexistence of stable low and high shear bands (A and B); (b) moderate coupling; (c) strong coupling. Squares show Hopf bifurcations. The thin black lines delimit the periodic orbit of the local model at fixed Σ .

microscopics of any given system. However, for concreteness we use the language of shear thinning WMs. There exist numerous reports of apparently unattainable homogeneous high shear rate branches in such systems, in which the sample flows erratically or is ejected from the cell (e.g., [1]). This is seldom discussed in detail, but sometimes attributed to surface instability. Nonetheless, the possibility of bulk instability remains. Indeed, in some WMs the high shear band breaks into subbands [26].

For simplicity we consider just one microstructural variable, the mean micellar length n , and define our model by

$$\Sigma = \sigma + \eta \dot{\gamma}, \quad (1)$$

$$\partial_t \sigma = -\frac{\sigma}{\tau(n)} + \frac{g[\dot{\gamma}\tau(n)]}{\tau(n)} + D \partial_y^2 \sigma, \quad (2)$$

$$\partial_t n = -\frac{n}{\tau_n} + \frac{N(\dot{\gamma}\tau_n)}{\tau_n}. \quad (3)$$

For simplicity we have restricted ourselves to a one-dimensional velocity $\mathbf{v} = \dot{\mathbf{x}}\mathbf{v}(y)$ with $\dot{\gamma}(y) = \partial_y v(y)$ in one spatial dimension y . Equation (1) gives the uniform shear stress $\Sigma(t)$ in the noninertial limit. It comprises a (generally nonuniform) viscoelastic micellar contribution $\sigma(y, t)$ and a solvent contribution with viscosity η . The dynamics of σ [Eq. (2)] has a length-dependent relaxation time [27]

$$\tau(n) = \tau_0 \left(\frac{n}{n_0}\right)^\alpha, \quad (4)$$

and a steady homogeneous state $\sigma = g[\dot{\gamma}\tau(n)]$ set by

$$g(x) = \frac{x}{1+x^2}, \quad (5)$$

admitting a constitutive curve of negative slope. The spatial gradients $D \partial_y^2 \sigma$ allow for a smooth interface of width $l \propto \sqrt{D}$ between the shear bands, and occur naturally in models where stresses arise from, e.g., spatial gradients of liquid crystalline orientation [8].

The micellar length n has its own relaxation time τ_n [Eq. (3)], related to the (unknown) underlying rates of micellar scission and recombination. For example, scission could be enhanced by the agitation of shearing or recombination aided by shear-induced alignment of micellar ends [22]. We assume the former, taking

$$N(x) = \frac{n_0}{1+x^\beta}. \quad (6)$$

Because this decrease sets in only for shear rates $\dot{\gamma} \geq 1/\tau_n$, the degree of coupling between the mechanical variables ($\Sigma, \sigma, \dot{\gamma}$) and length n can be tuned by varying τ_n .

Using this model we study flow between two parallel plates at $y = 0, L$ with boundary condition $\partial_y \sigma = 0$, using units in which $n_0 = 1$, $\tau_0 = 1$, and $L = 1$. We set $\alpha = 1.2$, $\beta = 1.5$, though our results are qualitatively robust to reasonable variations in these values.

Homogeneous dynamics.—The constitutive curves $\Sigma(\dot{\gamma})$ and domains of instability for homogeneous states under controlled stress are shown in Fig. 1. (At controlled strain rate, the system is unstable only to fluctuations with nonzero wave vectors $k > 0$: homogeneous instability, $k = 0$, is not possible.) For small $\tau_n \lesssim 0.115$ we find pure mechanical instability [Fig. 1(a)] that does not involve n . The constitutive curve is then (at any fixed Σ) an unstable saddle [28] (one unstable eigenvector). For larger τ_n , coupling to micellar length broadens this instability into the rising high shear branch, which is now an unstable focus [28] (two unstable eigenvectors): Figs. 1(b) and 1(c). This instability terminates in a Hopf bifurcation [28].

We then studied the nonlinear dynamics of the local ($D = 0$) model for fixed Σ , solving Eqs. (1)–(3) via a fourth order Runge-Kutte method [29]. This confirmed the stability properties of Fig. 1: states near an unstable (stable) segment of the constitutive curve flow away from (towards) that segment (Fig. 2). They also reveal a periodic orbit about the unstable high shear branch for stresses just below the Hopf bifurcation. We also used AUTO97 [30] to trace the amplitude of the periodic orbits, Figs. 1(b) and 1(c). Periodic orbits are the most complicated behavior possible for the local model since it has only two degrees of freedom, $d = 2$. Chaos requires $d \geq 3$ [28].

Spatially heterogeneous dynamics.—We now turn to the nonlocal model, $D \neq 0$, focusing on the implications of an unstable high shear branch [Figs. 1(b) and 1(c)]. The dimensionality d is now effectively infinite, since each spatial point has its own value of n and $\dot{\gamma}$. We solved the nonlocal equations using a Crank-Nicholson algorithm (checking our results with the Rosenbrock method) [29], with the constraint of fixed global strain rate, $\dot{\gamma} = \int_0^1 dy \dot{\gamma}(y, t)$. For small $\tau_n \lesssim 0.115$ we find stable shear bands [Fig. 1(a)]. In contrast, for $\tau_n = 0.145$ (unstable high shear branch) we find spatiotemporal oscillations and chaotic banded flows (Fig. 3).

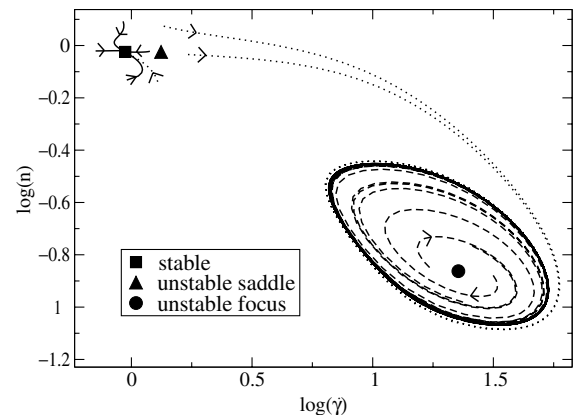


FIG. 2. Homogenous dynamics ($D = 0$) at fixed $\log \Sigma = -0.301$ for different initial conditions. $\tau_n = 0.145$.

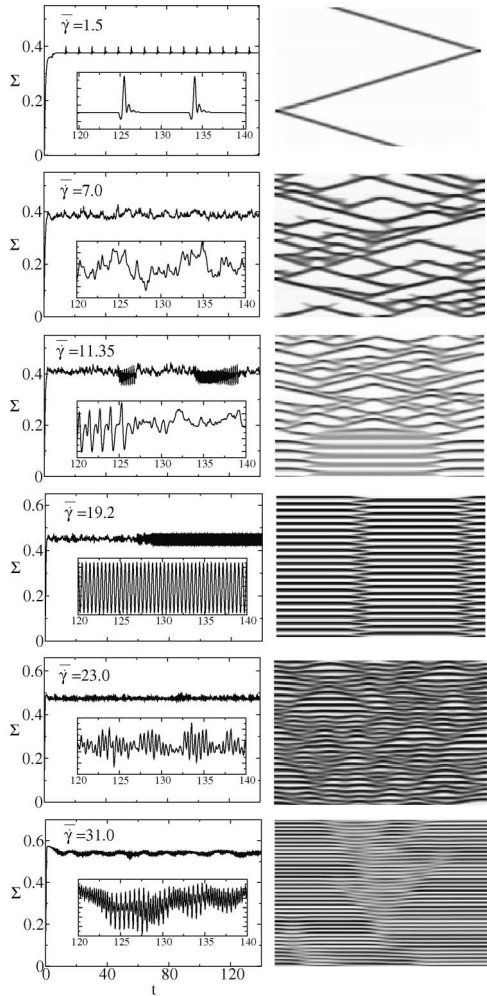


FIG. 3. Right: Space time plots for local shear rate evolution at applied global shear rate for $\tau_n = 0.145$, $D = 0.0016$ with space $y = 0-1$ left to right and time $t = 120-140$ bottom to top. In plots downward greyscale ranges are $\dot{\gamma} = 0.3-28.7$, $0.3-37.6$, $0.2-44.5$, $0.6-40.0$, $0.9-57.7$, and $8.7-58.1$. Left: corresponding stress versus time.

Several regimes are evident. At low applied shear, $\bar{\dot{\gamma}} = 1.5$, a thin pulse of high shear ricochets back and forth across the cell (Fig. 3, top). A thin fluctuating high shear band, away from the rheometer wall, was seen experimentally in Ref. [13]. At larger shear rates, we find two or more such pulses. For two pulses (not shown), we typically find a periodically repeating movie with the pulses alternately bouncing off each other (midcell) and the cell walls. Once three pulses are present, $\bar{\dot{\gamma}} = 7.0$, periodicity gives way to chaotic behavior (Fig. 3).

At still higher shear, $\bar{\dot{\gamma}} = 19.2$, we find regular oscillations of spatially extended bands pinned at stationary defects. The local shear rates span both the low and high shear constitutive branches. Oscillating (vorticity) bands were seen experimentally in Refs. [4,16]. For the intermediate value $\bar{\dot{\gamma}} = 11.35$ we find intermittency between patterns resembling those for $\bar{\dot{\gamma}} = 7.0$ and $\bar{\dot{\gamma}} = 19.2$.

Finally, for $\bar{\dot{\gamma}} = 23.0, 31.0$ we find oscillating bands separated by *moving* defects (Fig. 3, bottom right). The

flow is now governed only by the high shear constitutive branch. In each band, the shear rate executes the periodic orbit of the local model (Fig. 2 and top data set of Fig. 4).

The largest Lyapunov exponent (not shown) is positive, indicating chaos, in the multipulse ($2.5 \leq \dot{\gamma} \leq 10.5$) and defect dominated ($19.0 \leq \dot{\gamma} \leq 30.5$) regimes [31].

For different values of τ_n we find a host of other interesting phenomena [31]. For example, for weaker instability ($\tau_n = 0.13$) at low applied shear rates we see a high shear band that can pulsate in width while adhering to the rheometer wall [Fig. 5(a)] or can meander about the cell [Fig. 5(b)]. The former behavior resembles interfacial motion in seen WMs [14,15] and onion phases [11].

Finally, we discuss in more detail the results of Fig. 3 (top right), which show a high shear pulse traveling through a homogeneous phase on the low shear branch. At times when the pulse is far from the wall, the stress Σ is constant (flat regions in Fig. 3, top left). In this regime we transform to the pulse's comoving frame $\hat{y} = y - ct$ and eliminate $\sigma = \Sigma - \eta\dot{\gamma}$ to get

$$c\eta\dot{\gamma}' = -\frac{\Sigma}{\tau(n)} + \frac{g[\dot{\gamma}\tau(n)] + \eta\dot{\gamma}}{\tau(n)} - D\eta\dot{\gamma}'' \quad (7)$$

$$-cn' = -\frac{n}{\tau_n} + \frac{N(\dot{\gamma}\tau_n)}{\tau_n} \quad (8)$$

with constant parameters c and Σ . For a given Σ , there exists a single selected speed $c(\Sigma)$ for which Eqs. (7) and (8) allow a high shear rate pulse traveling through a low shear rate background (i.e., a “homoclinic orbit” connecting the low shear fixed point to itself). The corresponding global shear rate $\bar{\dot{\gamma}}(\Sigma) = \int_0^L dy \dot{\gamma}(y)$ then follows by integrating under this pulse. In fact, the results of Fig. 3 (top right) were obtained at fixed $\bar{\dot{\gamma}}$, with the system evolving to the stress given by the inverted relation $\Sigma(\bar{\dot{\gamma}})$. We used AUTO97 [30] to check that the homoclinic orbits of Eq. (8) coincide with these numerical

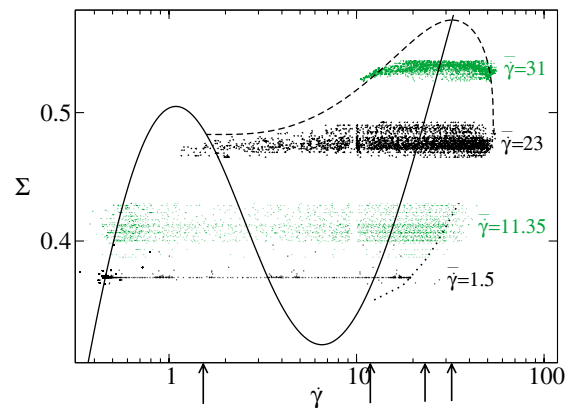


FIG. 4 (color online). Data of Fig. 3 for $\bar{\dot{\gamma}} = 1.5, 11.35, 23.0, 31.0$ (arrows under abscissa) and $130 < t < 140$ in condensed form. Solid line: intrinsic constitutive curve; long dashed line: extrema of the local periodic orbits; dotted line: maximum shear rate $\dot{\gamma}_n\sigma$ of the propagating high shear pulse described by Eqs. (8).

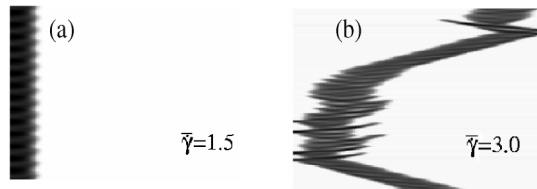


FIG. 5. Shear rate density plots for $\tau_n = 0.13$, $D = 0.0016$. Greyscale ranges are $\dot{\gamma} = 0.4\text{--}12.9$ (a); $\dot{\gamma} = 0.3\text{--}23.0$ (b).

results. The locus of the maxima $\dot{\gamma}_h(\Sigma)$ of these pulses is marked in Fig. 4. The data points for $\dot{\gamma} > \dot{\gamma}_h$ in Fig. 4 arise during wall collisions; correspondingly, their density is smaller than for $\dot{\gamma} < \dot{\gamma}_h$.

To summarize, we have constructed a simple model of shear banding in which the high shear branch of the underlying constitutive curve is rendered unstable by a coupling between flow and microstructure. Within this model, we have found a rich variety of spatiotemporal oscillatory and rheochaotic flows, many resembling experimental observations in shear banding systems. It remains an open challenge to delineate more fully the spectrum of mechanisms governing rheochaotic banded states. Extension to higher dimensions, allowing fluctuations along the plane of the interface would be interesting. Within the present one-dimensional approach, generalization to shear thickening systems [25], curved Couette geometries, and vorticity banding is under way [31].

We thank A. A. Aradian, P.T. Callaghan, M. E. Cates, E. Knobloch, A. M. Rucklidge, and J.-B. Salmon for interesting discussions, and EPSRC GR/N11735 for funding.

Note added.—After this paper was received, Chakrabarti *et al.* submitted a study of spatiotemporal chaos [32] in a model of liquid crystals that had been demonstrated to show temporal chaos in its local dynamics [19].

*Electronic address: s.m.fielding@leeds.ac.uk

- [1] M. M. Britton and P.T. Callaghan, Phys. Rev. Lett. **78**, 4930 (1997); J.F. Berret, G. Porte, and J.P. Decruppe, Phys. Rev. E **55**, 1668 (1997); V. Schmitt, F. Lequeux, A. Pousse, and D. Roux, Langmuir **10**, 955 (1994).
- [2] O. Diat, D. Roux, and F. Nallet, J. Phys. II (France) **3**, 1427 (1993).
- [3] E. Eiser, F. Molino, G. Porte, and O. Diat, Phys. Rev. E **61**, 6759 (2000).
- [4] L. Hilliou and D. Vlassopoulos, Ind. Eng. Chem. Res. **41**, 6246 (2002).
- [5] P. Sollich, F. Lequeux, P. Hébraud, and M. E. Cates, Phys. Rev. Lett. **78**, 2020 (1997).
- [6] J.S. Raynaud, P. Moucheront, J.C. Baudez, F. Bertrand, J.P. Guilbaud, and P. Coussot, J. Rheol. **46**, 709 (2002).
- [7] F. Varnik, L. Bocquet, J.L. Barrat, and L. Berthier, Phys. Rev. Lett. **90**, 095702 (2003).
- [8] P.D. Olmsted and P.M. Goldbart, Phys. Rev. A **41**, 4578 (1990); **46**, 4966 (1992).
- [9] N. A. Spenley, M. E. Cates, and T. C. B. McLeish, Phys. Rev. Lett. **71**, 939 (1993).
- [10] C.-Y. D. Lu, P.D. Olmsted, and R. C. Ball, Phys. Rev. Lett. **84**, 642 (2000).
- [11] J. B. Salmon, A. Colin, and D. Roux, Phys. Rev. E **66**, 031505 (2002); J.-B. Salmon, S. Manneville, and A. Colin, Phys. Rev. E **68**, 051503 (2003); L. Courbin, P. Panizza, and J.-B. Salmon, Phys. Rev. Lett. **92**, 018305 (2004).
- [12] R. Bandyopadhyay, G. Basappa, and A. K. Sood, Phys. Rev. Lett. **84**, 2022 (2000).
- [13] W.M. Holmes, M.R. López-González, and P.T. Callaghan, Europhys. Lett. **64**, 274 (2003).
- [14] M. M. Britton and P.T. Callaghan, Eur. Phys. J. B **7**, 237 (1999).
- [15] Y.T. Hu, P. Boltenhagen, and D.J. Pine, J. Rheol. **42**, 1185 (1998); R. Bandyopadhyay and A. K. Sood, Europhys. Lett. **56**, 447 (2001).
- [16] P. Fischer, E. K. Wheeler, and G.G. Fuller, Rheol. Acta **41**, 35 (2002).
- [17] H.M. Laun, J. Non-Newtonian Fluid Mech. **54**, 87 (1994); D. Lootens, H. Van Damme, and P. Hébraud, Phys. Rev. Lett. **90**, 178301 (2003).
- [18] M. E. Cates, D. A. Head, and A. Ajdari, Phys. Rev. E **66**, 025202 (2002).
- [19] M. Grosso, R. Keunings, S. Crescitelli, and P.L. Maffettone, Phys. Rev. Lett. **86**, 3184 (2001); G. Rienacker, A. Kroger, and S. Hess, Phys. Rev. E **66**, 040702 (2002).
- [20] J. Yerushalmi, S. Katz, and R. Shinnar, Chem. Eng. Sci. **25**, 1891 (1970).
- [21] S.M. Fielding and P.D. Olmsted, Eur. Phys. J. E **11**, 65 (2003); Phys. Rev. Lett. **90**, 224501 (2003).
- [22] M. E. Cates and M. S. Turner, J. Phys. Condens. Matter **4**, 3719 (1992).
- [23] M. Doi, J. Polym. Sci. Polym. Phys. Ed. **19**, 229 (1981); R.G. Larson, Macromolecules **23**, 3983 (1990); M. Grosso, S. Crescitelli, E. Somma, J. Vermant, P. Moldenaers, and P.L. Maffettone, Phys. Rev. Lett. **90**, 098304 (2003).
- [24] M. Kim, M. Bertram, M. Pollmann, A. von Oertzen, A.S. von Mikhailov, H.H. Rotermund, and G. Ertl, Science **292**, 1357 (2001).
- [25] A. A. Aradian and M. E. Cates, e-print cond-mat/0310660.
- [26] S. Lerouge, J.P. Decruppe, and J.F. Berret, Langmuir **16**, 6464 (2000).
- [27] F. Bautista, J.F.A. Soltero, J.H. Perez-Lopez, J.E. Puig, and O. Manero, J. Non-Newtonian Fluid Mech. **94**, 57 (2000).
- [28] S.H. Strogatz, *Nonlinear Dynamics and Chaos: with Applications to Physics, Biology, Chemistry and Engineering* (Addison-Wesley, Reading, MA, 1994).
- [29] W.H. Press, S.A. Teukolsky, W.T. Vetterling, and B.P. Flannery, *Numerical Recipes in C* (Cambridge University Press, Cambridge, 1992), 2nd ed.
- [30] E.J. Doedel, *AUTO97: Continuation and Bifurcation Software for Ordinary Differential Equations* (Concordia State University, Montreal, 1997).
- [31] S. M. Fielding and P.D. Olmsted (to be published).
- [32] B. Chakrabarti *et al.*, Phys. Rev. Lett. **92**, 055501 (2004).